



## STUDY OF THE HF SEISMIC ATTENUATION IN KINKI REGION, JAPAN, USING THE RAY THEORY ELASTIC ATTENUATION EFFECT IN 3-D VELOCITY MODEL AND THE 3-D STRUCTURE OF $Q$ -VALUE

Anatoly PETUKHIN<sup>1</sup>, Kojiro IRIKURA<sup>2</sup>, Takao KAGAWA<sup>3</sup>, Shiro OHMI<sup>4</sup>

### SUMMARY

We studied seismic waves attenuation in Kinki region, Japan, in high frequency range 1-10Hz. To do this it was assumed that observed amplitude Fourier spectrum is a product of source, elastic path attenuation, inelastic path attenuation and site effects. Inelastic path attenuation is described by the  $Q$ -value. Frequently, to estimate path attenuation effect,  $Q$ -value is inverted under simplified assumption that geometrical spreading is spherical. Actually, elastic attenuation is complex effect that includes geometrical spreading in non-uniform velocity model, reflection and conversion on major velocity discontinuities, free-surface effect. In this study, elastic path attenuation was calculated using the ray-theory approach in 3-D velocity model. Source and Site effects were eliminated using the double-spectral ratio scheme. Travel times inside blocks were calculated by the 3-D ray tracing. After this,  $Q$ -values in blocked media were inverted using a tomography approach. For this study, we developed 3-D velocity model for Kinki area. This model includes: low-velocity layer (LV), upper crust (UC), lower crust (LC), subducted Philippine Sea plate (SP) and mantle wedge (MW). The whole media of the wave propagation were divided into blocks with constant  $Q$ -value according to the tectonic structure. For inversion we used borehole data of the Hi-net and Denkyoken networks and hard rock/stiff soil data of CEORKA network. Analysis of the results of inversion shows that largest  $Q \sim 150f^{0.8}$  was in UC block, smallest  $Q = 70f^{0.57}$  was in LC+MW block; for SP  $Q = 175f^{0.3}$ . In UC,  $Q$ -value is larger in central Kinki region:  $Q = 220f^{0.86}$ , than in the south:  $Q = 120f^{0.55}$  or in northern part of Kinki region:  $Q = 125f^{0.68}$ . Based on results of inversion we calculated examples of attenuation correction factor: the difference between path attenuation calculated by the developed model and by the uniform model, for a set of sources.

### INTRODUCTION

To increase accuracy of strong ground motion prediction, it is necessary to develop method to estimate  $Q$ -value based on realistic model of geometrical spreading. Using such method we can try to estimate nonuniform, especially depth dependent  $Q$ -value. The result would let to develop a model of path attenuation of seismic waves, which gives more reliable extrapolation to target distances.

---

<sup>1</sup> Geo-Research Institute, 4-3-2 Itachibori, Nishi, Osaka, 550-0012 Japan. Email: anatoly@geor.or.jp

<sup>2</sup> Disaster Prevention Research Institute, Kyoto University, Japan

<sup>3</sup> Geo-Research Institute

<sup>4</sup> Disaster Prevention Research Institute

In this study, we developed a method of attenuation tomography inversion and estimated  $Q$ -value structure in Kinki region on this base. To estimate  $Q$ -value, at first step it is necessary to eliminate effect of elastic attenuation (mainly geometrical spreading). Results for both  $Q$ -value and distance attenuation depends on the method of elimination used. In this study, for high-frequency range ( $f > 1\text{Hz}$ ) we employ the ray approximation and calculated elastic attenuation using the ray-theory. For this purpose, we used the Complete Ray Tracing (CRT) method of Červený [1] both for calculation of elastic attenuation and for ray tracing. Another feature of the developed method is the using of the double-spectral ratio method in tomography inversion to reduce trade-off between source (and site) effect and  $Q$ -value.

Seismicity of the studied region consists of the shallow crustal earthquakes 0-18km depth (upper crust seismogenic layer) and deep subduction zone earthquakes 20-70 km depth located in the Philippine Sea subducted plate (Philippine slab), dipping under  $45^\circ$  in the northwest direction under the Eurasia plate. Lower crust and mantle wedge between them have no earthquakes (aseismic zone). Because Philippine slab is young and thin (around 30 km), its shape is strongly distorted (undulating, wavy). Due to this, velocity structure in studied region is essentially three-dimensional.

For this work we developed original 3-D velocity model in Kinki region that was compiled from available information: seismicity data, travel-time tomography results, seismic exploration results, gravity data and borehole measurements. Based on the case study of 4 types of velocity structure, velocity model that has strong gradient inside each layer was selected for analysis. It was assumed also that in high frequency range, at a point of crossing with velocity interface there is no reflection/conversion for upward rays. Data used in the inversion are the high-frequency (1 – 10Hz) data of CEORKA and Hi-net networks.

Results of this study are a structure of  $Q$ -value specific for Kinki region and corresponding attenuation model. This study continues our study of  $Q$ -value in Kinki region for 1-D case (Petukhin [2]) and through the text we frequently will make references to this earlier work.

## METHOD OF DOUBLE-SPECTRAL RATIO TOMOGRAPHY INVERSION

In the method of spectral inversion (Iwata [3]), observed amplitude spectrum  $O(f)$  is modeled as the product:

$$O = S \cdot \left( \frac{\rho_0 v_0}{\rho v} \right)^{1/2} \cdot g \cdot \exp\left(-\pi \frac{Rf}{vQ(f)}\right) \cdot G \cdot \varepsilon, \quad (1)$$

where:  $S(f)$  - source effect,  $g$  – path elastic attenuation, exponential function - path inelastic attenuation,  $G(f)$  – site effect,  $\varepsilon$  - random error term,  $\rho$  and  $\rho_0$  – density at source and site respectively,  $v$  and  $v_0$  – wave velocity for source and site. For a set of data of several earthquakes recorded simultaneously at several sites, after taking logarithm of both parts of equation (1), it is possible to estimate parameters  $S$ ,  $G$  and  $Q$  by linear inversion. As was shown in Petukhin [2], due to presence of the  $\varepsilon$  term, in this method there is a possibility for trade-off between source + site effect and  $Q$ -value (trade-off with source effect is stronger than with site effect). To reduce effect of this trade-off, in this study we employ the double-spectral ratio approach, see Chun [4]. Following equation (1), taking double-spectral ratio of 4 spectra (corrected for the seismic impedance term) from 2 sources  $i$  and  $j$  observed at 2 sites  $n$  and  $m$ , according to equation below, eliminates source and site effects.

$$DSR = \frac{O'_{in} \cdot O'_{jm}}{O'_{im} \cdot O'_{jn}} = \frac{g_{in} \cdot g_{jm}}{g_{im} \cdot g_{jn}} \cdot \exp\left(-\pi \frac{R_{in} - R_{im} + R_{jm} - R_{jn}}{v} \cdot \frac{f}{Q}\right) \cdot c^\varepsilon, \quad (2)$$

where

$$O' = O \cdot \left( \frac{\rho v}{\rho_0 v_0} \right)^{1/2}. \quad (3)$$

Elimination of source and site effects before inversion reduces possibility of the trade-off with  $Q$ -value.

After reducing equation (2) for the preliminarily calculated elastic attenuation term, and taking logarithm of both parts of equation we have simple linear equation that can be used in attenuation tomography inversion. Final equation used in the inversion is (for notations see Figure 1):

$$\log DSR'_{ijmm} = -\pi \sum_k \frac{R_{in}^k - R_{im}^k + R_{jm}^k - R_{jn}^k}{v^k} \cdot \frac{f_l}{Q^k} + \varepsilon_{ijmm}, \quad (4)$$

where

$$DSR'_{ijmm} = DSR_{ijmm} \cdot \frac{g_{im} g_{jn}}{g_{in} g_{jm}}. \quad (5)$$

In equation (4) unknown parameters are  $Q$ -values in blocks denoted by superscript  $k$ . Figure 1 illustrate the developed procedure.

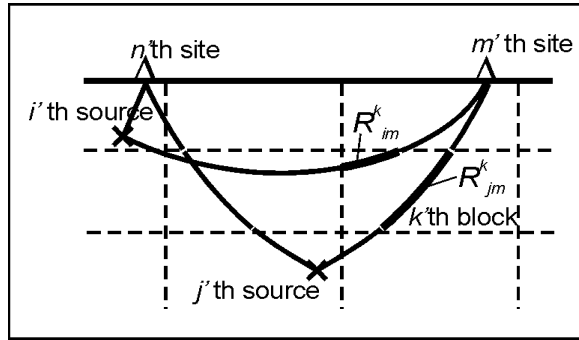


**Figure 1. Scheme illustrating the modified double-spectral ratio tomography inversion procedure, see equation (4). Dashed lines – blocks, solid lines – rays, bold paths are the paths with constant  $Q = Q^k$ .**

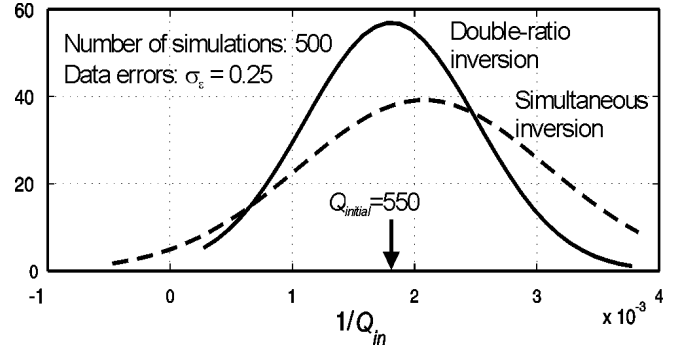


**Figure 2. Distribution of inversion results of the artificial data sets, simulated by equation (1). Dashed line - using regular spectral inversion method, solid line - using developed double-spectral ratio method. Arrow indicates initial  $Q$ -value.**

We should mention here, that in the basic double-spectral ratio method (Chun [4]), to reduce effects of source radiation pattern and/or azimuth dependence of site effect, location of sources and sites usually are selected in specific way: pairs of sources and sites are located on the same straight line. In our case such strict criteria for selection strongly reduce data available for analysis and make tomography inversion impossible. From another hand, even if the pairs of sources and sites are located according to selection criteria of the method, possible effects of the radiation directivity of source radiation (due to high speed of rupture propagation) and of the incident angle dependence of site effect and effects of the seismic scattering, are adding noise to  $DSR$  values. Another fundamental source of additional noise in the  $DSR$  is

that if each component of the *DSR* has random error with standard deviation  $\sigma_\varepsilon$ , random error of *DSR* itself will have standard deviation  $2\sigma_\varepsilon$ . This additional noise is negligible in the double-difference travel-time tomography, but become important in the attenuation tomography, where  $\sigma_\varepsilon$ -value related to the observed values is large. In our method we prefer to increase double-spectral ratios data set many times using free criterion for selection and all possible combinations of source-site pair's *ijnm*. We expect that in such approach effect of increasing of number of data will overcome effect of increasing of noise and will make inversion more stable.

In example on Figure 2, we made numerical experiment and inverted 500 different data sets, simulated by equation (1) for simple case of uniform velocity and  $Q$  structure, using regular spectral inversion method and the developed double-spectral ratio method, and then fitted the inversion results for  $Q$ -value by Gauss (normal) distribution. Results show, that using the double-spectral ratio method reduces standard deviation of inverted  $Q$ -values 1.5 – 2 times and reduce shift of the average inversion result.

Additionally, similarly to Petukhin [2], to reduce possible trade-off between  $Q$ -value in seismogenic layer and  $Q$ -values in another blocks we used a two-step layer-stripping algorithm.

1. At the first step, only data of shallow events, whose rays pass within the upper seismogenic layer, were used to estimate  $Q$ -structure in the upper crust.
2. At the second step, data of events from the subduction zone deeper than 20 km were used. In this case, the rays pass through both the upper crust and lower crust + mantle wedge + slab. To determine  $Q$  in the deeper part we fixed  $Q$  in the shallow part using results of the first step of inversion.

## VELOCITY MODEL

The velocity model for Kinki-region was constructed from 6 blocks/layers: (1) uppermost low-velocity layer, (2) seismogenic layer (upper crust), (3) lower crust, (4) Philippine slab, (5) mantle wedge and (6) upper mantle, see Figure 3 for the bird's-eye view and Figure 4 for the cross-section perpendicular to the subduction zone through the central part of studied region. This model was compiled from next data.

1. First is the seismicity data. Following results of Nakamura [5], we defined the upper boundary of the Philippine slab. Lower boundary of the seismogenic layer was specified following to the study of inland seismicity by Ito [6]. In this study, we assumed that this is also boundary between upper and lower crust (Conrad interface).
2. Second are seismic tomography results for S-velocity. Here we used results of Zhao [7] and constructed velocity models for the upper crust, lower crust and mantle wedge. Although Zhao [7] also estimated the upper boundary of the Philippine slab and the Conrad surface position, we prefer more detail results of seismicity studies, because, as was shown in Petukhin [2], location of velocity interfaces can be critical for estimation of  $Q$ -value. To specify lower boundary of the crust (Moho interface) we used results of Zhao [7].
3. Third data is the results of deep seismic profiling. The results of Kamei [8] (see also Kodaira [9]) were used to specify S-wave velocity structure in the Philippine slab. We consider that results of Kamei [8] are more reliable for this part than results of Zhao [7], because in Kamei [8] amplitude data were used together with the travel time data. Particularly, the existence of a low-velocity layer in upper part of slab (see Fig. 4) was proved by unusually large reflection from the slab boundary.
4. The fourth and fifth data sets are gravity anomaly data and exploration data. In Petukhin [2] it was found that existence of the shallow low-velocity layer interface is critical for estimation of  $Q$ -value in the seismogenic layer. In this study, we try to develop more detail 3-D structure of low-velocity layer in a simplified way using available information. For this we assume that in studied region, relatively far from the plate margin, deep underground structure is uniform. In this case, variations of the gravity anomaly field can be correlated with the depth of low-velocity layer. Using gravity anomaly data (Bouguer anomaly) and correlating them with available seismic profiling results for shallow structure, the 3-D structure of the depth of the low-velocity layer was estimated. Estimated correlation between the Bouguer

anomaly value and the depth of low-velocity layer is shown in Table 1. Such simplified procedure let us to construct realistic 3-D structures under deep sedimentary basins, like Osaka basin or Biwa Lake basin, see upper interface in Figure 3. Borehole measurements of S-velocity at Hi-net sites were used to fix velocity on the upper boundary of the low-velocity layer.

**Table 1. Assumed correlation between value of Bourguer anomaly and the depth of low-velocity layer.**

Bouguer anomaly, mGal	Depth of low-velocity layer, km
40	1.0
24	1.5
16	2.0
8	3.0
-8	4.0
-24	6.0

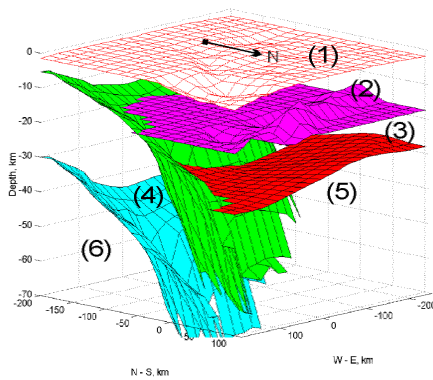


**Figure 3. Bird's-eye view of the velocity model used in this study. Numbers: (1) low-velocity layer, (2) seismogenic layer (upper crust), (3) lower crust, (4) Philippine slab, (5) mantle wedge and (6) upper mantle.**

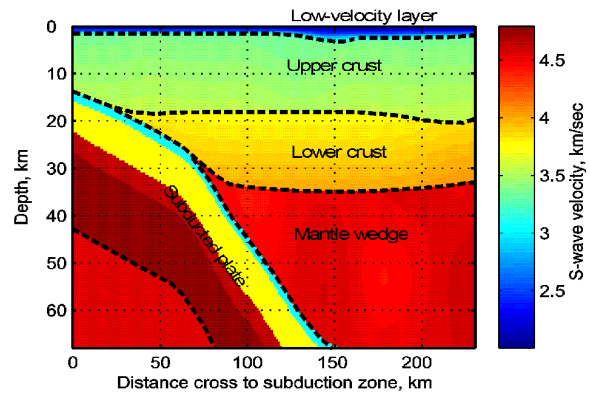


**Figure 4. Cross-section of the 3-D velocity model (type 3, see Figure 6 below), perpendicular to the subduction zone and passing through the central part of studied region.**

### Validation of the velocity model

To check the compiled 3-D velocity model we calculated P-wave travel times and compare them with observed travel times. CEORKA data were used for this analysis. Results are shown on Figure 5 for model type 4 (see below). Analysis of the figure show that the difference between observed and calculated P-arrivals is small: smaller than +/- 1 sec, and average difference is smaller than standard deviation of residual values. This indicates that compiled model hasn't large systematic errors and it is acceptable for analysis. From another hand, a noticeable trend exists in average plots: with increasing distance, average residual between observed and calculated travel time increases. In feature work, it is necessary to correct velocity model and remove this effect. The type 4 model gives smaller average residuals than other models. Note that average relative error of the travel time is almost zero for shallow events and is only around 1% for deep events.

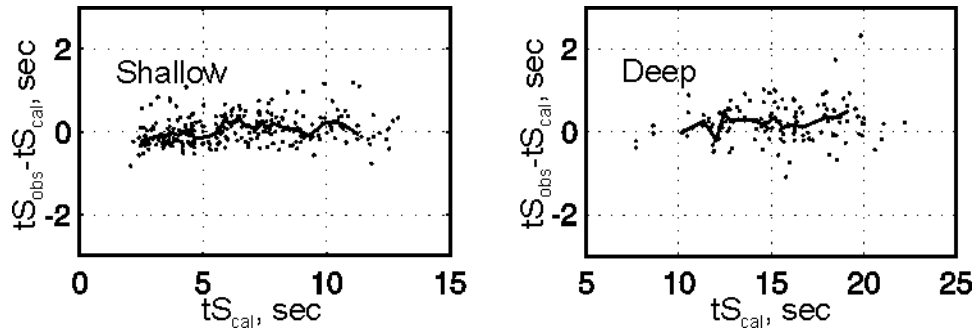


**Figure 5. Validation of the compiled 3-D velocity model. Residuals between observed and calculated P-arrival time (points) are plotted versus P-wave travel time. Results for type 4 model. Left subplot – seismogenic layer, shallow events, right subplot – subduction zone, deep events. Line is the average trend.**

### Velocity interpolation in layers

During calculation of the elastic attenuation (Petukhin [2]), we run into next problem. Seismic tomography or seismic exploration results, which are based on the travel time data only, frequently are presented as step-like velocity models. Actually, for calculation of elastic attenuation, velocity gradients in layers and the structure of transition zones between layers become important. In this work, to perform a case study, we considered 4 types of velocity models, see Figure 6.

1. General step-like model. For this kind of model, because the seismic rays are the straight lines, incident angles to interface become large and elastic attenuation due to reflection and refraction becomes strong.
2. Step-like model + linear velocity gradient inside layers. In this model incident angle become smaller, but due to existence of the velocity discontinuity, effect of reflection losses still exists.
3. Model 2 + interfaces with a wide transition zone between layers. In this case, we expect minimal effect of reflection from interface due to the absence of velocity discontinuity. We should say that at high frequencies with short wavelength, physically, this kind of model makes sense.
4. Gradient velocity model. In the last model, effect of the ray diving is the largest and this reduces effect of refraction but increase length of ray.

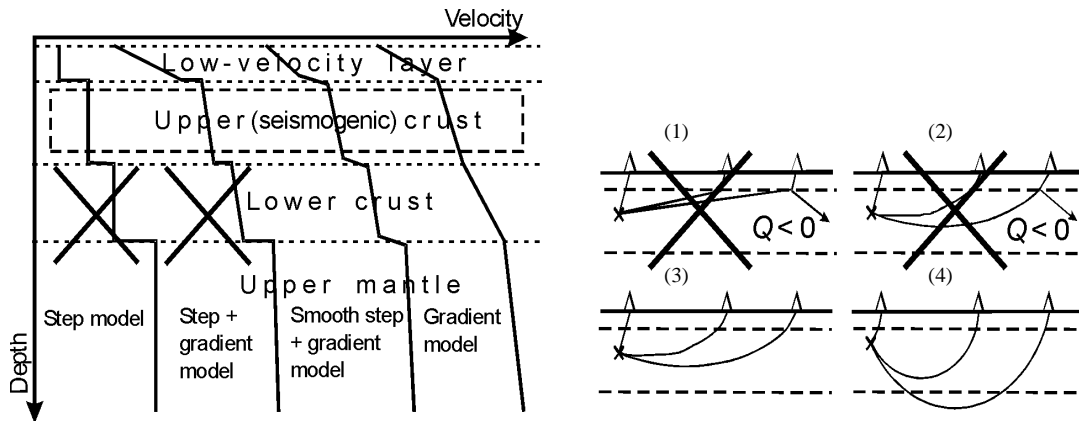


**Figure 6. Types of the velocity interpolation used in this analysis (left figure). (1) General step-like model. (2) Step-like model + linear velocity gradient inside layers. (3) Type 2 model + interfaces with a wide transition zone between layers. (4) Gradient velocity model. Ray diagrams (right figure) are shown for each type of model (see comments in text).**

Results for models 1 and 2 show negative values for  $Q$ . We rejected them. Results for models 3 and 4 are similar, but because scattering of residuals of the spectral amplitudes and average residuals of the travel time are slightly smaller for model 4, below we consider results only for model 4.

### Tomography blocks

Structure of tomography blocks was constructed following to the next assumptions.

1. Blocks must be large enough. There are two reasons for this. First, to solve ill conditioned attenuation tomography inversion problem, ray coverage for each block (number of rays crossing this block) should be large. Second, the size of block should be several times larger then the width of the scattered, physical ray. For details, see discussion in Petukhin [2].
2. For large blocks, better results are expected if the structure of blocks will coincide with tectonical structure in the studied region or expected  $Q$ -structure.
3. For the upper crust blocks, natural boundaries between blocks are the major faults in the studied area, which are also bound tectonically uniform subregions.

Figure 7 shows assumed structure of blocks. Upper crust/seismogenic layer is divided into 6 blocks. The boundaries between blocks are the major fault systems in the Kinki region. These are: Median Tectonic Line (MTL), Nojima fault, Arima-Takatsuki Tectonic Line (ATL), Yamazaki fault, Mitoke fault, Hanaori fault and fault system along West boundary of Nara valley. Comparison of the assumed block structure for upper crust with geological structure shows good correlation: block 1 is tectonically depressed block under Osaka basin; block 2 is composed mostly from Late Cretaceous rhyolite and dacite rocks; block 3 – Permian to Jurassic shale of Tamba group; block 4 (southern part, covered by rays) – composed from Late Cretaceous granite; block 5 – accretion prism; block 6 – depression of Seto Inland Sea (see Hashimoto [10]).

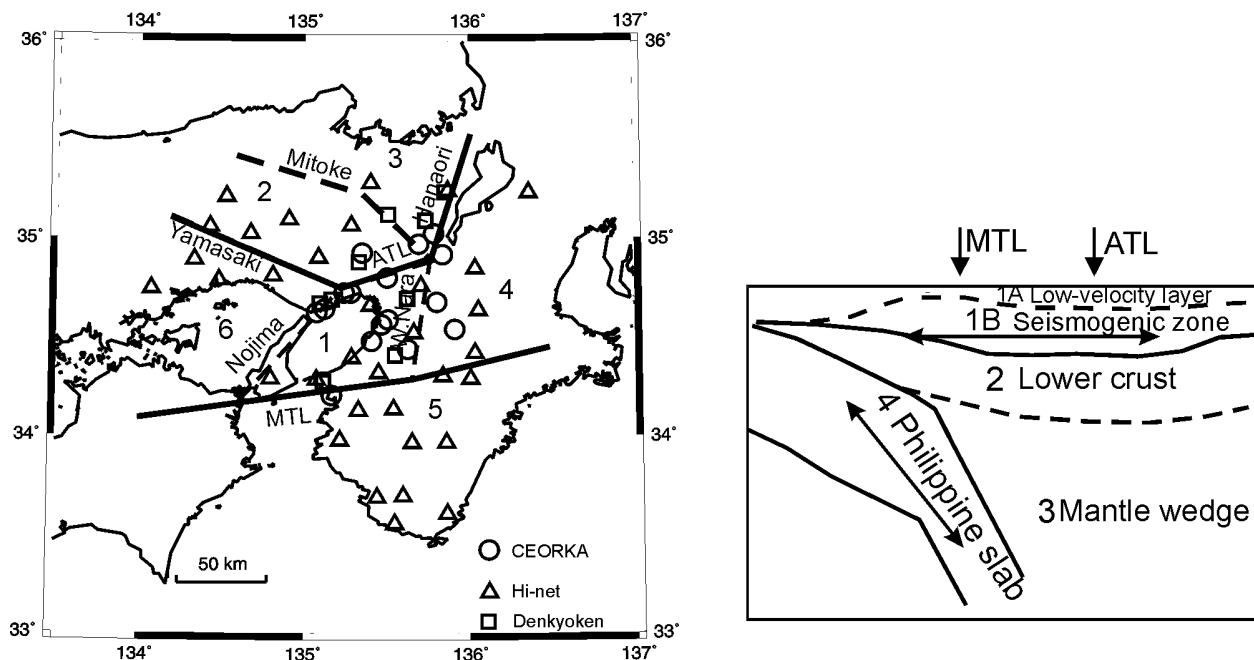


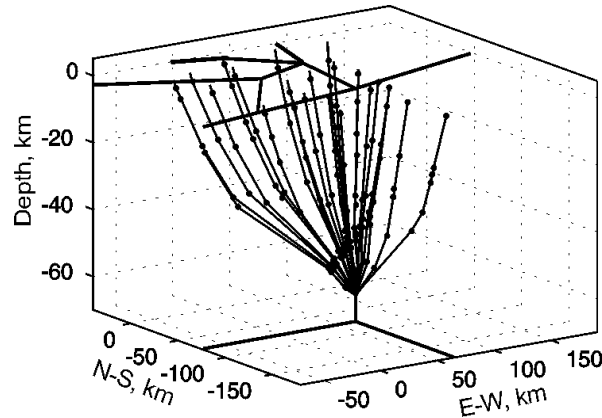
**Figure 7. Assumed structure of blocks. Left figure: block structure for upper crust. Right figure: block structure for lower part of the medium. Double arrows approximately indicate location ranges of used earthquakes. On left figure, locations of observation sites used in the analysis are also shown.**

Model volume below upper crust was divided into 3 blocks: lower crust, mantle wedge and Philippine slab. Low-velocity layer above the seismogenic layer was considered as one additional block. On the same figure, observation sites used in the analysis are plotted.

## DATA PROCESSING

In this work, we used mostly the same data set of the Hi-net data as in Petukhin [2] slightly enlarged by the data of local networks CEORKA (Committee for the Earthquake Observation and Research in Kansai Area) and Denkyoken (managed by 11 electric companies of Japan). Data selection criteria and processing are also almost the same. Instead of using complicated procedure for selection of the direct S-wave time window, which was based on the polarization analysis, in this work we used simple, 3sec window (Moya [11]). This value is around 2-3 times larger than in previous work; we prefer it because for most records it covers the main amplitude segment, which is important for engineering applications. Total number of records is 1453.

For ray tracing and for calculation of elastic attenuation we used the Complete Ray Tracing package (CRT5.3) of Červený [1]. For the purpose of this study we made few modifications of the distributed code: (1) obtain block number along the ray; (2) obtain material parameters (velocity and density) in the starting point of the ray; (3) to model interfaces with a transition zone, a version with fixed reflection coefficient equal 0.0 and transmission coefficient equal 1.0 were developed. Figure 8 shows example of ray tracing for one deep event in subduction zone.



**Figures 8.** Bird's-eye view of ray tracing for a sample subduction zone event. Point marks along the rays show points of crossing of ray with an interface. Lines on ground surface are scheme of blocks.

### Calculation of elastic attenuation

To analyze elastic attenuation it is convenient to use parameter  $n$ , which was calculated according to equation:

$$g = 1/R^n \Rightarrow n = -\frac{\log g}{\log R} \quad (6)$$

For example,  $n = 1.0$  corresponds to spherical geometrical spreading,  $n = 0.5$  – cylindrical geometrical spreading,  $n < 1.0$  indicates focusing effect and  $n > 1.0$  indicates defocusing effect.

To calculate exponent of elastic attenuation  $n$  using equation (6), at first parameter  $g$  was calculated using CRT method from equation:

$$A = \sqrt{A_{SV}^2 + A_{SH}^2} = \sqrt{\frac{\rho_0 \cdot v_{S0}}{\rho \cdot v_S}} \cdot \sqrt{g_{SV}^2 + g_{SH}^2} = \sqrt{2} \cdot \sqrt{\frac{\rho_0 \cdot v_{S0}}{\rho \cdot v_S}} \cdot g, \quad (7)$$

where  $g$  – elastic attenuation,  $A$  – RMS ray theory amplitude of two horizontal components (calculated by the CRT),  $\rho$  and  $\rho_0$  – density at source and site respectively,  $v_S$  and  $v_{S0}$  – S-wave velocity at source and site. Parameter  $R$  (length of ray) in equation (6) also is calculated by the CRT.

Values of parameter  $n$ , calculated for developed 3-D velocity model, are shown on Figure 9a and 9b. In case of shallow earthquakes, in average,  $n$ -value increase with increasing of the epicentral distance from value 0.97 in the epicentral region to 1.1-1.2 at a large distances. At the same epicentral distance,  $n$ -value increases with decreasing of depth. In case of deep earthquakes, similar effect of increasing of  $n$ -value also exists but the absolute value is much smaller.

Tendency to increase with increasing of epicentral distance on Figure 9a is caused by the refraction on the shallow velocity interface/boundary of low-velocity layer (in case of model 1-3 on Figure 6, see Petukhin [2]), or arise from the increasing of length of ray due to diving effect (in case of model 4), or both. Results for  $n$ -value on Figure 9b don't show clear dependency vs. distance and depth, because for deep earthquakes incident angle to interface is small and refraction is negligible, and because diving effect for subvertical rays is small.

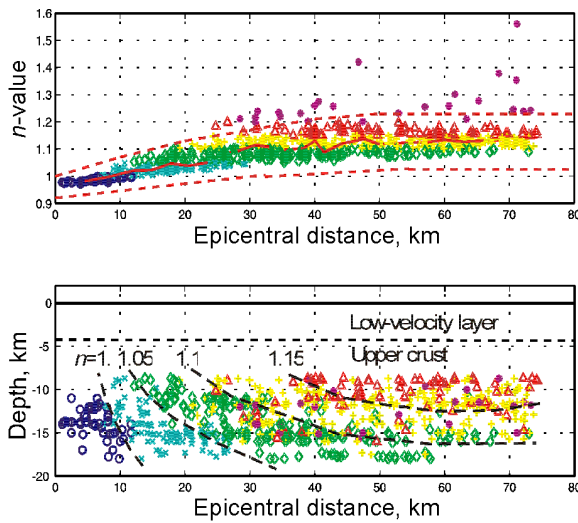


**Figure 9a.** Parameter  $n$  calculated by CRT for developed 3-D velocity model, upper crust events. Upper figure plots  $n$ -value vs. epicentral distance. Circles, crosses, diamonds, pluses, triangles and stars indicate data in different ranks:  $n < 1.0$ ,  $1.0 \leq n < 1.05$ ,  $1.05 \leq n < 1.1$ ,  $1.1 \leq n < 1.15$ ,  $1.15 \leq n < 1.2$  and  $1.2 \leq n$  respectively. Solid line – average trend, dashed lines bounds data used in analysis. Lower figure shows distribution of the same data vs. depth and epicentral distance, dashed lines approximately indicates boundaries between data of different ranks.

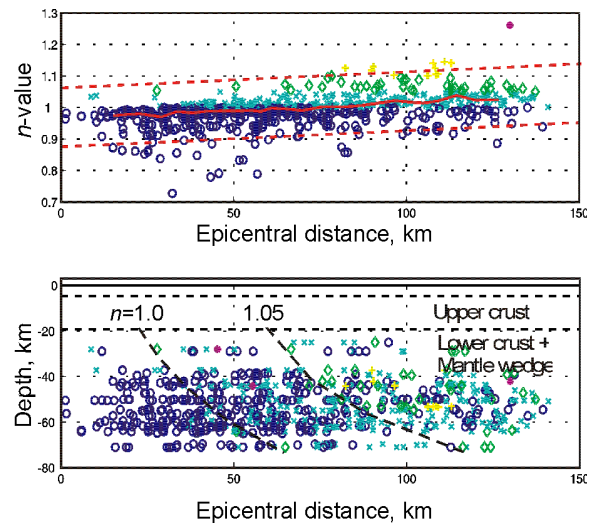


**Figure 9b.** Parameter  $n$  calculated by CRT for developed 3-D velocity model, subduction zone events. Notations are the same as in previous figure. Note weak dependence of  $n$ -value vs. depth and epicentral distance.

For some records, calculated  $n$ -values become anomalously large or small (outliers). Probably this is due to inconsistency of the developed 3-D velocity model for some particular ray traces. We rejected such data with  $n$ -values above and below the red dashed lines on Figure 9a and 9b.

### RESULTS OF INVERSION

Direct using of calculated elastic attenuation results in negative  $Q$ -value in some blocks in wide frequency range. We consider these estimations physically unreasonable and reduced elastic attenuation in the following way:

$$n_c - 1 = (n - 1) / 2 , \quad (8)$$

where  $n_c$  – exponent of corrected elastic attenuation. Probable reason, why such correction is necessary, is the effect of reflections from the lower crust reflectors, which was neglected in our analysis. In future study, this effect should be modeled and considered in an accurate way.

Results of inversion are shown on Figure 10 and Table 2. Inversion results for block structure on Figure 7 were unstable in some blocks. To stabilize them we combined blocks in upper crust with numbers 1, 4 and 6 on Figure 7a, north of the MTL, into one block, and blocks with number 2 and 3 in northern part of Kinki into another block. Also, for the same reason we had to combine lower crust and mantle wedge (blocks 2 and 3 on Figure 7b) into one block. Analysis of Figure 10 and Table 2 shows that largest  $Q \sim 150f^{0.8}$  was in upper crust block, smallest  $Q = 70f^{0.57}$  was in lower crust + mantle wedge block; for Philippine slab  $Q = 175f^{0.3}$ . In upper crust,  $Q$ -value is smaller in area south from the MTL:  $Q = 120f^{0.55}$ , than in area north from the MTL:  $Q = 125f^{1.7}$  for  $f < 4$  and  $Q = 1000$  for  $f > 4$ . In northern part of Kinki region average value is  $Q = 125f^{0.68}$ .

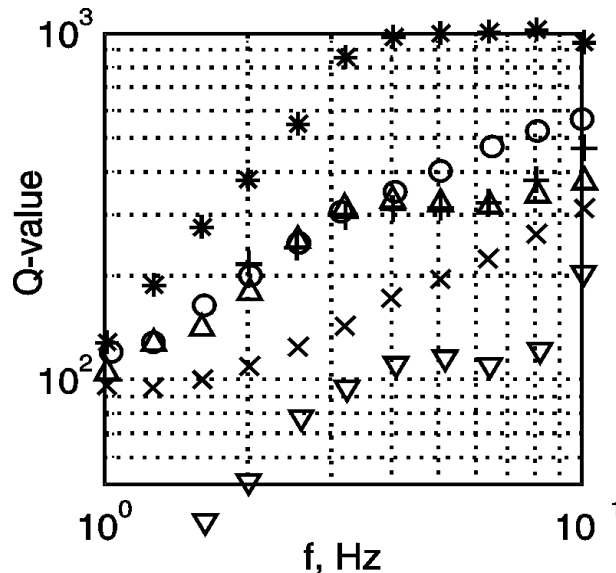


**Figure 10. Results of inversion for  $Q$ -value: upper crust, north of MTL (stars), upper crust, south of MTL (triangles), Northern Kinki (circles), lower crust + mantle wedge (crosses), Philippine slab (pluses), low-velocity layer (reverse triangles).**

Higher  $Q$ -value for upper crust was expected from our previous analysis (Petukhin [2]). Lower  $Q$ -value in lower crust and mantle wedge is supported by another observation: many low-frequency earthquakes were detected near junction of Eurasia crust and Philippine slab, from the mantle wedge side (Obara [12]).

This indicates partial melting in this corner, which also has to result in higher attenuation and lower  $Q$ -value. Although not stable (we don't show it here), result of our inversion for  $Q$ -value in the lower crust and mantle wedge separately, shows tendency to have lower  $Q$  in lower crust than in mantle wedge. The observation that  $Q$ -value in slab is higher than in the neighborhood is consistent with the results of some other studies of attenuation, for example Mori [13] and with results of velocity tomography Zhao [7].

**Table 2. Results of  $Q$ -value inversion.**

	Upper Crust			Lower Crust + Mantle Wedge	Philippine slab	Low-Velocity Layer
	North of MTL	South of MTL	Northern Kinki			
Q-value	$125f^{1.7}$ ( $f < 4$ ) $1000$ ( $f > 4$ )	$120f^{0.55}$	$125f^{0.68}$	$70f^{0.57}$	$\sim 175f^{0.3}$	$\sim 25f^{0.9}$

We also tried to estimate  $Q$ -value in the low-velocity layer. In spite of expected strong trade-off between  $Q$ -values in low-velocity layer and upper crust (distribution of ray pass length in low-velocity layer is strongly nonuniform due to subvertical incidence of rays), results for  $Q$ -value are reasonable and comparable with results of other studies (Hough [14], Abercrombie [15], Satoh [16]).

### PATH ATTENUATION RELATIONS

In next step, we calculated examples of the path attenuation relations, using the inverted  $Q$ -structure, and elastic attenuation  $g$  calculated for the developed 3-D velocity model. To do this we selected six sources in one vertical plane, crossing subduction zone and passing through the center of studied region. Two sources are in the upper crust: one is near MTL at depth 10 km and another is near the southeast edge of studied region at depth 15 km. Another 4 sources are located in Philippine slab at depths 35, 45, 55 and 60 km. Receivers were located on the line of intersection of this plane with the surface. Results for all sources at  $f = 4$  Hz are plotted on Figure 11.

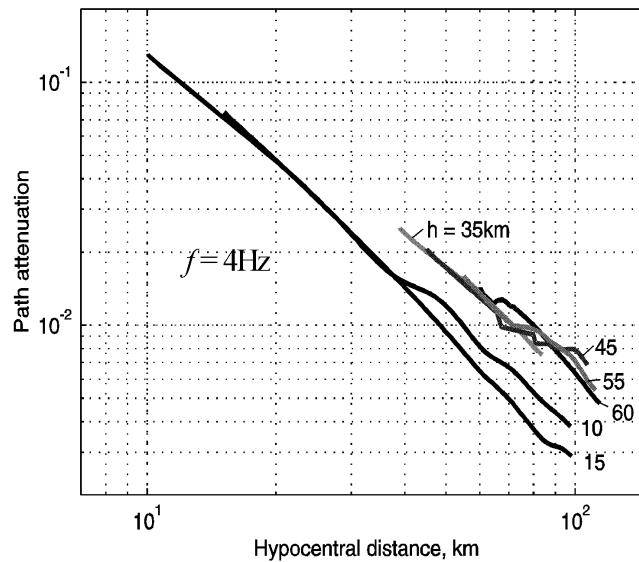


**Figure 11. Examples of the path attenuation relations,  $f = 4$  Hz.**

Calculated attenuation relations have next features.

1. For the same hypocentral distance deep earthquakes have smaller attenuation than shallow earthquakes. This is due to larger effect of elastic attenuation for shallow earthquakes than for deep earthquakes. Effect of elastic attenuation is stronger than effect of  $Q$ -value. The last one, conversely, is larger ( $Q$ -value is smaller) for deep earthquakes.
2. Attenuation along part of the observation line above Osaka basin is smaller (amplitude is larger). For example see hump on plot with  $h = 10$  km at distances  $R > 40$ km. This is due to focusing effect in the bottom of Osaka basin structure.

To understand, how our 3-D attenuation model differ from regular uniform attenuation model, we introduce correction factor as follows:

$$C_{cor}(f) = \log\left(\frac{A_{3-D}}{A_{unif}}\right), \quad (9)$$

where  $A_{3-D}$  – spectral amplitude from a unit point source in 3-D velocity and  $Q$  structure,  $A_{unif}$  – spectral amplitude from the same point source in the uniform structure. For prediction of strong ground motions, such correction factor can be applied to the results of prediction that are based on the uniform structure.

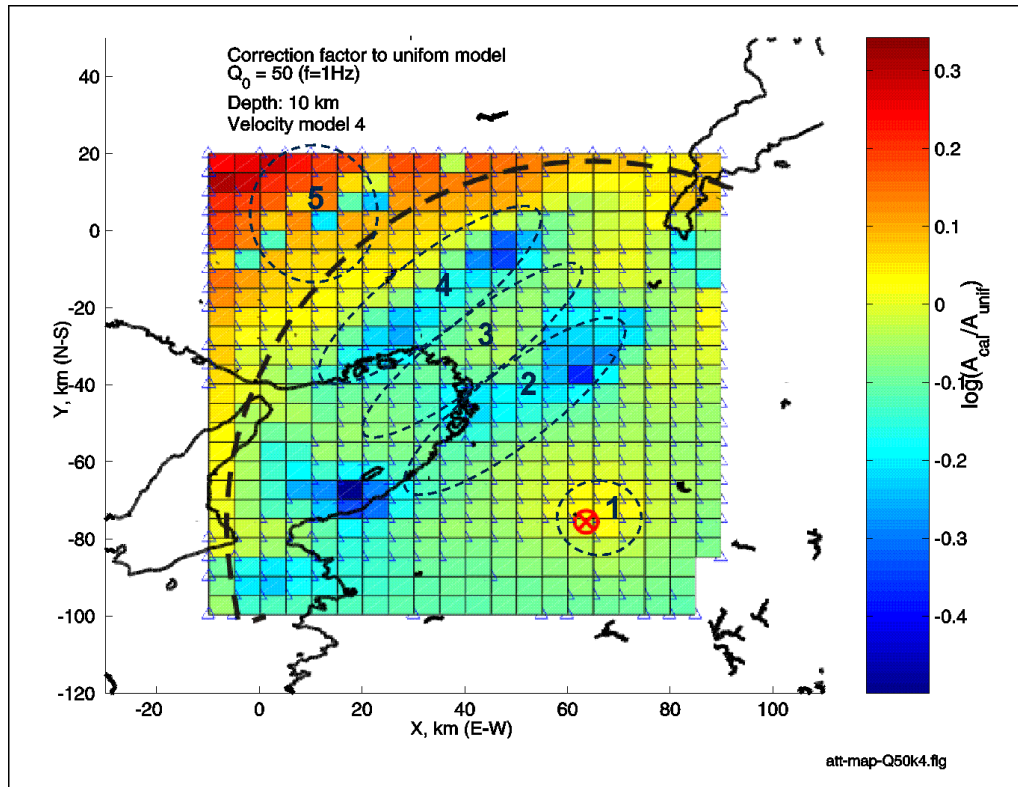


**Figure 12. Map of calculated correction factor  $C_{cor}$  to the uniform attenuation model with  $Q = 50$  ( $f = 1$  Hz). Red cross – epicenter of source, source depth is 10 km. Zones 1 – 5 correspond to different types of geometrical spreading, see text for details. Thick dashed line shows the 75 km limit of applicability of the developed attenuation model.**

We used the 10km depth point source located near the MTL line to calculate an example of the correction factor  $C_{cor}$  at  $f = 1$  Hz. Map on Figure 12 shows the result. To calculate  $A_{3-D}$  we used developed 3-D velocity model (type 4) and inverted  $Q$ -structure. To calculate  $A_{unif}$  we assumed  $Q(1\text{Hz}) = 50$ ; average

level of the path attenuation curve in this case approximately coincide with the average level of 3-D attenuation curve. Generally, attenuations for the uniform and 3-D models are similar: variations of  $C_{cor}$  are not large: from  $-0.3$  to  $+0.15$ . However, we should mention, that good fit is the result of proper selection of the uniform  $Q$ -value, adjusted to the location of point source. For another point source, another best-fit uniform  $Q$ -value is expected. If we will assume the same uniform  $Q$ -value for all sources,  $C_{cor}$  will be larger.

In Figure 12, systematic changes are visible in some zones. For zones marked by numbers from 1 to 5 analysis of rays show, that geometrical ray spreading patterns are different: zone 1 - focusing of upgoing rays in the low-velocity layer; zone 2 - defocusing on the nearest edge of Osaka basin; zone 3 - focusing in the bottom of Osaka basin structure; zone 4 - defocusing on the opposite edge of Osaka basin (weak shadow effect); zone 5 - decreasing of the refraction effect in low-velocity layer for diving rays (actually this zone is already in a region where the generation of  $L_g$  waves is expected and CRT approach is not applicable).

## CONCLUSIONS

1. Results of inversion confirm previous results with 1-D velocity model of Petukhin [2]:  $Q$ -value in seismogenic layer is noticeably larger than  $Q$ -value in aseismic layer.
2.  $Q$ -value inside Philippine slab has larger value than mantle wedge and lower crust at the same depth.
3. Effect of reflective lower crust can be large and should be included into calculation of the elastic attenuation.
4. Examples of the distance attenuation relations are calculated. They show that errors of uniform attenuation model due to simplification can be large.

Acknowledgements. Many thanks to consortium "Seismic Waves in Complex 3-D Structures", project leader Vlastislav Červený, for providing CRT package. We also deeply appreciate the National Institute of Earth Science and Disaster Prevention for providing the Hi-net data, the CEORKA research society and the Joint Research Program of the 11 electric power companies of Japan, for using their strong ground motion data.

## REFERENCES

1. Červený V, Klimens L, Pšenčík I. "Complete seismic-ray tracing in three-dimensional structures." Doornbous DJ, editor. Seismological algorithms. New York: Academic Press, 1988.
2. Petukhin A, Irikura K, Ohmi S, Kagawa T. "Estimation of  $Q$ -values in the seismogenic and aseismic layers in the Kinki region, Japan, by elimination of geometrical spreading effect using ray approximation." Bull.Seismol.Soc.Am., 2003; 93: 1498-1515.
3. Iwata T, Irikura K. "Source parameters of the 1983 Japan sea earthquake sequence." J.Phys.Earth., 1988; 36: 155-184.
4. Chun K-Y, West GF, Kokoski RJ, Samson C. "A novel technique for measuring  $L_g$  attenuation: results from Eastern Canada between 1 to 10 Hz." Bull.Seismol.Soc.Am., 1987; 77: 398-419.
5. Nakamura M, Watanabe H, Konomi T, Kimura S, Miura K. "Characteristic activities of subcrustal earthquakes along the outer zone of Southwestern Japan." Annuals of Disas. Prev. Res. Inst., Kyoto Univ., 1997; No. 40 B-1: 1-20 (in Japanese).
6. Ito K. "Seismogenic layer, reflective lower crust, surface heat flow and large inland earthquakes." Tectonophysics, 1999; 306: 423-433.
7. Zhao D, Hasegawa A, Kanamori H. "Deep structure of Japan subduction zone derived from local, regional and teleseismic events." J.Geophys.Res., 1994; 99B: 22313-22329.
8. Kamei Y. "Seismic velocity structure of an area surrounding Kii peninsula." Master thesis, Kobe university 1996 (in Japanese).

9. Kodaira S, Takahashi N, Park J-O, Mochizuki K. "Western Nankai Trough seismogenic zone: Results from a wide-angle ocean bottom seismic survey." *J.Geophys.Res.*, 2000; 105B: 5887-5905.
10. Hashimoto M. "Geology of Japan." Tokyo: Terra Scientific Publishing Company, 1991.
11. Moya A, and Irikura K. "Attenuation and site effect in the Osaka area, Japan." Irikura K, Kudo K, Okada H, Sasatani T, editors. *The effects of surface geology on seismic motion; recent progress and new horizon on ESG study*. Rotterdam : AA Balkema, 1998: vol. 2, 469-474.
12. Obara K. "Nonvolcanic deep tremor associated with subduction in Southwest Japan." *Science* 2002; 296: 1679-1681.
13. Mori J. "Estimates of the attenuation in the Philippine Sea plate slab using strong motion data from the 2001 Geiyo earthquake." ABSTRACTS 2002 Japan Earth and Planetary Science Joint Meeting, CD-ROM: S042-006.
14. Hough SE, Lees JM, Monastero F. "Attenuation and source properties at the Coso geothermal area, California." *Bull.Seism.Soc.Am.* 1999; 89: 1606-1619.
15. Abercrombie R. "Crustal attenuation and site effects at Parkfield, California." *J.Geophys.Res.* 2000; B105: 6277-6286.
16. Satoh T. "Inversion of  $Q_s$  of sediments from vertical array seismograms using simulated annealing method." XXIII General Assembly of the International Union of Geodesy and Geophysics 2003. Abstracts: SS04a/09P/D042, p.B503.